Crystallography and reorientation mechanism upon deformation in the martensite of an α-α' Ti-6Al-4V dual-phase microstructure exhibiting high work-hardening rate

O. Dumas[a,b], L. Malet[a], B. Hary[a], F. Prima[b], S. Godet[a]

[a] 4MAT, Université Libre de Bruxelles, 50 Avenue F.D. Roosevelt (CP 165/63), 1050, Bruxelles, Belgium

[b] PSL Research University, Chimie ParisTech, CNRS, Institut de Recherche de Chimie Paris, 75005, Paris, France

Keywords

Ti-6Al-4V
Work-hardening
Martensite
Crystallography
Self-accommodation
Reorientation

Abstract

The present study provides a fundamental understanding of the crystallography and the microscale behavior of the V-enriched and Al-depleted α' martensite taking place during the microstructure formation and the deformation of the dual phase α + α' microstructure produced in Ti-6Al-4V. This particular microstructure exhibits much larger work-hardening capabilities than the conventional wrought product. The as-quenched structure

of the martensite is analyzed using the Phenomenological Theory of the Martensite Crystallography (PTMC) coupled with EBSD analyses. This approach sheds new light on the microstructure configuration obtained during the dual-phase treatment and its fine-scale mechanical behavior. The martensite preferentially forms into parallel groups of 3 self-accommodating variants separated by a misorientation of $63.26°/[\overline{10}\ 5\ 5\ \bar{3}]_{\alpha'}$. TEM analyses additionally show that the variants of a same group are separated by a hitherto unobserved $\{13\bar{4}1\}_{\alpha'}$ type twin plane. Post-mortem analyses after tensile testing demonstrate that this twinning plane is mobile under deformation. This allows the martensitic microstructure to exhibit the remarkable property to reorient under uniaxial tension. This unique property is shown to be intimately related to the mobility of the $\{13\bar{4}1\}_{\alpha'}$ twinning plane thereby evidencing for the first time that twin boundary motion is not uniquely associated to the orthorhombic α'' martensite but can also occur in hexagonal α' martensite. Quantification of the Interaction Energy (IE) appears relevant to rationalize and predict the reorientation of the martensite. The critical influence of the parent β grains texture on the reorientation is evidenced, while the impact of this deformation mechanism on the ductility of the martensite is debated.

1. Introduction

Titanium alloys and Ti-6Al-4V in particular, are widely used in the aerospace for their excellent mechanical strength to density ratio and high corrosion resistance [1]. However, the relatively low work-hardening capabilities of these alloys compared to other metals like steels still restricts their usage [2]. This limited work-hardening is associated with a low uniform strain (typically in the order of 10% [3]) and a high sensitivity to strain localization [2]. Moreover, increasing the work-hardening is an efficient way to improve

the toughness and the damage tolerance of metallic alloys. Indeed, during ductile fracture, the growth and coalescence of the cavities will be influenced in the first order by the hardening capacity of the material between the growing defects. The improvement in the work-hardening rate is therefore an important challenge for the development of titanium alloys with an enhanced toughness, energy absorption ability and damage tolerance [4–6]. Already crucial for structural applications, the damage tolerance criterion becomes particularly critical in 3D printed parts since fabricated alloys contain unavoidable randomly distributed defects inherent to the process, leading to early damage and fracture upon loading. de Formanoir et al. [7] recently reported that sub-transus annealing treatments followed by water quenching generate a dual-phase microstructure that offers a wide range of mechanical properties. The associated microstructure is a mixture of vanadium-depleted and aluminum-enriched alpha phase (α) and vanadium-enriched and aluminum-depleted martensite (α'). The latter is a particularly complex phase characterized by an extremely large number of interfaces between neighboring variants of acicular martensitic plates. The respective volume fraction of each phase as well as their grain size and chemical composition can be modified by varying the annealing temperature in the α+β field. A remarkably high work-hardening rate coupled with an interesting balance between strength and ductility was obtained when both phases were formed in similar volume fractions. The improvement of the work-hardening capabilities was attributed to the kinematic hardening that arises from the mechanical contrast between the α and α' phase. Indeed, the V-enriched and Al-depleted α' phase was found to be the first phase to yield and to deform to a larger extent than the α phase [8–10]. This behavior differs significantly from the dual-phase steels widely used in the automotive sector [11]. In that case, the carbon enriched α' martensite is much harder than the ferrite

phase [12]. This finding also challenges the conventional ideas about α' martensite. Indeed it is usually reported to be a hard and brittle phase when formed from the *β-phase field* in Ti-6Al-4V alloy [13-14]. As referred in [3][7][9][15-16], the V content of the β phase significantly increases and the Al content decreases when the annealing temperature in the *α+β phase field* decreases. It is worth noting that this compositional change results in a decrease in the c/a ratio for the quenched α' martensitic phase. Similarly, Matsumoto et al. [14] recently argued that such a change in its chemical composition could partly explain the large room temperature ductility of α' martensite when it is quenched from low temperature (850°C-900°C). Indeed, the aluminum-depletion is suspected to bring a gradual change in the dislocations organization that goes from a heterogenous deformation substructure with dislocations that are arranged in planar configurations to a homogeneous deformation substructure with dislocation lines that exhibit a straight characteristic. This change triggers a progressive increase in the ductility of the martensite. A planar configuration promotes the pile ups of dislocations on a single slip plane that lead to a great decrease in the amount of plasticity achieved by the material [17-18]. Another characteristic reported in martensitic transformations is the need of self-accommodation between martensite plates that is required to minimize the transformation strain of the system [19]. From the above, it is clear that there is a lack of fundamental understanding of the crystallography and mechanical behavior of the V-rich and Al-poor α' martensite present in the dual-phase microstructure. The aim of the present paper is to provide further insight into the microstructure developments at play during the dual-phase treatments in Ti-6Al-4V and into the fine-scale mechanical behavior of martensite during tensile testing.

2. Experimental methods

A Ti-6Al-4V alloy manufactured by TIMET Savoie was used. It was forged, hot rolled in the α + β field, annealed at 730°C and finally machined to a 20mm diameter section. The chemical composition of the final bar is reported in Table 1. Its characteristics are in accordance with AMS4928 [20].

Table 1 Chemical composition of the as received Ti-6Al-4V alloy (wt%)

Al	V	Fe	O	C	N	Y
6.32	4.12	0.19	0.19	0.008	0.004	<0.0004

100mm long cylinders were cut from the as-received bars and encapsulated into quartz tubes filled with Argon. A dual-phase microstructure composed of about 40% of α' martensite was obtained by annealing for 2h at 880°C and quenching in water by breaking the capsules. The volume fractions of the α and α' were determined by using quantitative Rietfel refinement of XRD data and further confirmed by image analysis. The chemical composition of the two phases were measured by using a XFlash® 6T | 60 Bruker EDX system attached to a Tecnai G^2 20 S-TWIN TEM operated at 200kV. The heat-treated specimens were then machined to cylindrical tensile specimens characterized by a uniform section of 26mm in length and 4.5mm in diameter. Machining also allowed the thin oxidation layer formed during the heat treatment to be removed.

The tensile specimens were deformed until fracture at a cross-head speed of 5.10^{-4} s^{-1} using a Zwick Roell Z100 tensile testing machine.

Specimens from the head (undeformed) and from the gauge length away from the necking region (uniformly deformed) of the tensile specimens were cut perpendicularly to the

tensile axis and conventionally prepared for metallographic inspection. The final polishing step was carried out with a solution of colloidal silica. Back-scattered electron (BSE) images were obtained on a ZEISS LEO 1530 FEG-SEM. EBSD measurements were performed on a Hitachi SU70 FEG-SEM operated at 15kV and equipped with a Hikari® CCD camera. A step size of 40nm was used. The analysis of the EBSD measurements was carried out using TSL® OIM analysis™ software. The reconstruction of the orientation of the prior β grains was performed using an in-house software whose algorithm is described in Appendix A. 1.

Thin foils for TEM examination were cut from the head of the tensile specimen and mechanically ground down to a thickness of about 80µm. 3mm diameter discs punched from this plate were further electro-polished by the twin-jet method using a solution consisting of 95% of methanol and 5% of sulfuric acid at 20V and -40°C. TEM observations were performed on a FEI/Philips CM-20 operated at 200kV. Automated crystal orientation measurements (ACOM) were carried out using the ASTAR® system.

3. Parameters of the PTMC calculation

A complete description of the crystallography of the α' titanium martensite was conducted in the framework of the Phenomenological Theory of the Martensite Crystallography (PTMC) of Bowles and Mackenzie [21]. This theory associates a unique shape strain matrix to each of the 12 variants that are generated during the phase transformation from the body-centered cubic (bcc) parent β phase to the hexagonal close packed (hcp) daughter or product α' martensite. This association allows to rationalize the preferential formation of particular clusters of variants in a similar manner to that originally proposed by Bokros and Parker [22] in their seminal study of the mechanical couplings between

variants of martensite in an iron-based alloy. The full PTMC calculation was performed using PTCLab Software with the following hypotheses [23]. The lattice correspondence between the bcc and hcp structures obtained from the Bain strain was used [24]. The lattice parameters of both phases were taken as a_β=3.3065 Å for β and, $a_{\alpha'}$=2.95 Å, $c_{\alpha'}$=4.686 Å for α' as measured by Wang et al. [25]. The choice of the lattice invariant shear (LIS) was more delicate since TEM observations show that the internal substructure of α' martensite contains either dislocations or twins [3]. However, Wang et al. [25] showed that the nature of the clusters of variants was independent from the choice of the LIS. That the nature of the LIS does not significantly affect the crystallography of Ti martensite stems from the marginally small magnitude of the shear associated with the LIS needed to ensure an invariant plane. PTMC calculations show that this magnitude is m2=0.00517, that is two order of magnitude smaller than the total shape deformation. Hence, for the present study, the LIS was chosen to occur on dislocation glide on $\{110\}\langle\bar{1}11\rangle_\beta$ to be able to compare the results with those of Wang et al. [25] who had already carried out a complete PTMC computation with this LIS. The crystallographic predictions for each variant are reported in Appendix A. 2. The Orientation Relationship (OR) is found to be only 0.5° away from the exact Burgers OR. Owing to this small difference, each variant will be referred to its corresponding closest Burgers variant. The predicted Habit planes (HP) are only 2.3° away from $(334)_\beta$ which is commonly reported for α' titanium martensite [26]. The direction of the shape strain (D) is also reported in Appendix A. 2. The magnitude of the shape deformation was calculated to be m=0.2. Based on these features, the shape strain of a specific variant i (Sv_i) is estimated as follows in Eq. 1[27]:

$$S_{V_i} = I + m * HP_{V_i} * D_{V_i}^T \quad \textbf{Eq. 1}$$

Where I is the identity matrix.

4. Experimental results

4.1. *Description of the as-quenched α' martensite of the Ti-6Al-4V dual-phase microstructure*

4.1.1. The morphology and variant groupings of as-quenched α' martensite

Fig. 1 is a SEM image of the α + α' dual-phase microstructure formed after quenching from 880°C. Globular α grains, enriched in aluminum (6.3±0.2wt%) and depleted in vanadium (2.3±0.2wt%), appear dark. Their average diameter is about 10±2μm. The brighter phase corresponds to the vanadium-enriched (6.8±0.1wt%) and aluminum-depleted (4.5±0.1wt%), α' martensite. Using SEM, only the larger martensite plates can be distinguished, and their maximum width is about 300nm.

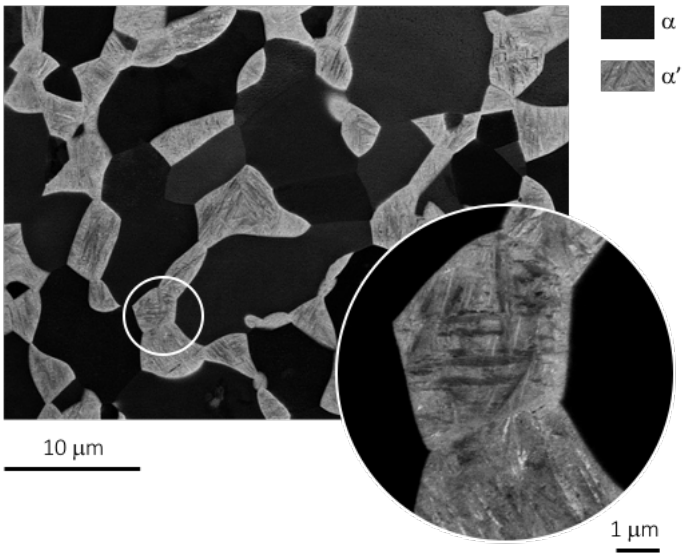

Fig. 1 BSE micrograph of the α (dark phase) - α' (bright phase) dual-phase microstructure.

Fig. 2 is a TEM bright field micrograph of the α + α' dual-phase microstructure formed after quenching from 880°C. The martensite exhibits a typical acicular morphology containing $\{10\bar{1}0\}_{\alpha'}$ transformation twins and stalking faults. It is also observed that the martensite form parallel plates that all have the same length. This organization differs from the hierarchical organization of the martensite formed from the β-phase field or the martensite of a dual-phase microstructure quenched at higher temperature (typically 950°C) [14][28]. In that case indeed, coarse (1st generation) as well as fine (2nd generation) variant cohabit in the microstructure.

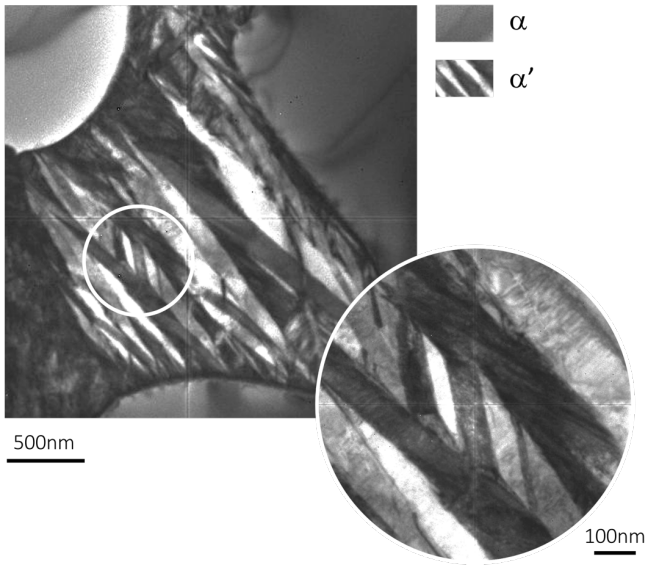

Fig. 2 TEM bright field micrograph of the α + α' dual-phase microstructure formed after quenching from 880°C

The crystallography of the α' martensite of the dual-phase microstructure formed after quenching from 880°C was studied in detail by means of EBSD. Fig. 3a is the Inverse Pole Figure (IPF) map of the α' martensite. The plates of α' martensite form groups of parallel variants. The variants correspond to different orientations of the well-known

Burgers Orientation Relationship (OR) [29]: $\{101\}_{\beta} \parallel \{0001\}_{\alpha'}$ and $\langle \bar{1}11 \rangle_{\beta} \parallel \langle 11\bar{2}0 \rangle_{\alpha'}$, that take place during the displacive phase transformation from the high temperature bcc β phase to the hcp room temperature α' martensite. It can be shown that there are only 5 possible misorientations between the 12 possible variants of the Burgers OR that could form from each parent β grain [30]. These misorientations are described as angle/axis pairs in Table 2.

Table 2 5 possible axis/angle misorientations between the 12 variants of the Burgers OR that could form from each parent β grain

Angle/axis pairs
$\mathbf{10.53°/[0001]}_{\alpha'}$
$\mathbf{60°/[11\bar{2}0]}_{\alpha'}$
$\mathbf{60.83°/[-1.377, -1, 2.377, 0.359]}_{\alpha'}$
$\mathbf{63.26°/[\overline{10}\ 5\ 5\ \bar{3}]}_{\alpha'}$
$\mathbf{90°/[1, -2.38, 0.359, 0]}_{\alpha'}$

Yet, the experimental distribution of intervariant misorientations observed in the α' martensite of the dual-phase microstructure differs noticeably from that theoretically expected from a random arrangement of variants [30]. More precisely, among the 5 possible misorientations that can take place between the variants, only the two intervariant boundary misorientations of $63.26°/[\overline{10}\ 5\ 5\ \bar{3}]_{\alpha'}$ and $60°/[1\ 1\ \bar{2}\ 0]_{\alpha'}$ are mainly observed (see Fig. 3a) . Moreover, the one at $63.26°/[\overline{10}\ 5\ 5\ \bar{3}]_{\alpha'}$ has a fraction which is 3 times larger than the one at $60°/[1\ 1\ \bar{2}\ 0]_{\alpha'}$ (0.40 compared to 0.14). Such a selection of misorientations has already been reported in pure Ti and its alloys, but in this case,

both misorientations (60° and 63.26°) were found to be present in similar proportions [30].

Fig. 3b is a map of the reconstructed prior β grains using the algorithm described in Appendix A. 1. Using a set of reconstructed prior β grains maps, the average diameter of the prior β grains was estimated at 5µm.

Knowing the parent β orientation allows a unique variant number to be associated to each α' martensite plate. In Fig. 3c, a color gradient scheme is used to identify and track the variants.

Comparison of Fig. 3b and c shows that each prior β grain is mostly transformed into one group composed of 3 variants that are separated by a specific misorientation, namely $63.26°/[\overline{1}0\ 5\ 5\ \bar{3}]_{\alpha'}$ (as grain n°1, 2 and 3). The other prior β grains (4, 5 and 6) are transformed into several groups composed of 3 variants. In this case, the same specific misorientation at $63.26°/[\overline{1}0\ 5\ 5\ \bar{3}]_{\alpha'}$ is observed between the variants of the same group whereas a misorientation at $60°/[1\ 1\ \bar{2}\ 0]_{\alpha'}$ takes place between two groups. Misorientation analysis shows that 4 such groups of 3 variants separated by a misorientation of 63.26° can be formed among the 12 variants of the Burgers OR. To identify these groups, a shade of the same color and a letter from A to D are attributed in Appendix A. 2 to the variants that belong to the same group. In order to rationalize the preferential formation of these 4 particular clusters of variants, the shape strain matrix of each variant defined in Eq. 1 is used. The *average* shape strain matrix of the variants V_1, V_5 and V_8 reads:

$$\frac{S_{V_1} + S_{V_5} + S_{V_8}}{3} = \begin{bmatrix} 0.99 & 0.01 & -0.01 \\ 0.01 & 0.99 & -0.01 \\ -0.01 & -0.01 & 0.99 \end{bmatrix} \approx I$$

The average shape strain matrix of the 3 variants that compose a group gives a result very close to the identity matrix. In other words, each parent β grain is mostly transformed into one or more groups of 3 variants misoriented by $63.26°/[\overline{10}\ 5\ 5\ \bar{3}]_{\alpha'}$ that can mutually compensate their respective shape strains. Such clusters of variants that are able to minimize the transformation strains are referred to as self-accommodating plate groups. Using PTMC on pure Ti, Wang et al. [25] calculated the average shape strain matrices of all the possible groups of 3 and 4 variants that could form among the 12 possible variants. They identified two different families of groups composed of 3 variants that can mutually compensate their shape strains. Each of these two families of groups is fully characterized by a unique misorientation between their variants. The first family, referred as Self-Accommodating Plate Group (SAPG) 1 in the following, is defined by a misorientation of $63.26°/[\overline{10}\ 5\ 5\ \bar{3}]_{\alpha'}$ and corresponds to the groups form in the present study. Each group is identified in Appendix A. 2 by a letter from A to D. For example, V_1, V_5 and V_8 pertain to SAPG 1B. The second family, referred to as SAPG 2 is defined by a misorientation of $60°/[1\ 1\ \bar{2}\ 0]_{\alpha'}$. In the present study, this misorientation is found to be much less frequent. Indeed, it can be seen from Figure 2a that this second misorientation can be observed in two cases. In a first case, it takes place between adjacent martensite variants pertaining to two neighboring priors β grains. In the second case, it is found between two adjacent martensite plates pertaining to neighboring SAPG 1s. However, no groups composed of three variants misoriented by $60°/[1\ 1\ \bar{2}\ 0]_{\alpha'}$ can be observed in the present microstructure.

Fig. 3d is the $\{334\}_{\beta}$ pole figure of the habit planes of the variants formed in grain 1. It can be seen that the habit planes (HP) of the variants of the same SAPG 1 are about 14° away from each other and gather around the same $\{111\}_{\beta}$ plane of the prior β grain. These

results are consistent with the observation that the variants of the same SAPG 1 are almost stack in parallel. An example is shown in Fig. 2d, where the projected traces of the HPs of the variants formed in grain 1 correspond closely to the long dimension of the plates and are all approximately parallel. Although various authors [25][31] have predicted *theoretically* that the SAPG 1 configuration offers the best possible accommodation among possible groups of variants that could form during the β to α' transformation, it had, to the author's knowledge, never been observed *experimentally* before the present study. Indeed, 63.26° misorientation has been reported so far to be one of the two misorientations predominantly taking place between two variants without forming complete SAPG 1s composed of 3 variants [30]. As shown in pure Ti using a stereological procedure, Beladi et al. [30] showed that the intervariant boundary plane associated with a misorientation at $63.26°/[\overline{10}\ 5\ 5\ \bar{3}]_{\alpha'}$ and thus, in our case, associated to a SAPG 1, is close to $(4\bar{1}\bar{3}0)_{\alpha'}$. However, the limited resolution of their method (about 10°) did not provide a definitive assessment of the nature of this interface plane. At this stage of the analysis and since the variants of the same SAPG 1 adopt a parallel morphology, it can be added that this intervariant boundary plane between these variants should be close to the $\{334\}_{\beta}$ habit plane (see Fig. 3d).

To summarize, α' variants formed in the dual-phase microstructure are mostly clustered into self-accommodating plate groups of type 1 which are characterized by an intervariant misorientation of $63.26°/[\overline{1}0\ 5\ 5\ \overline{3}]_{\alpha'}$. It remains therefore to characterize the nature of the intervariant interface associated with this particular misorientation. This is the aim of the following section.

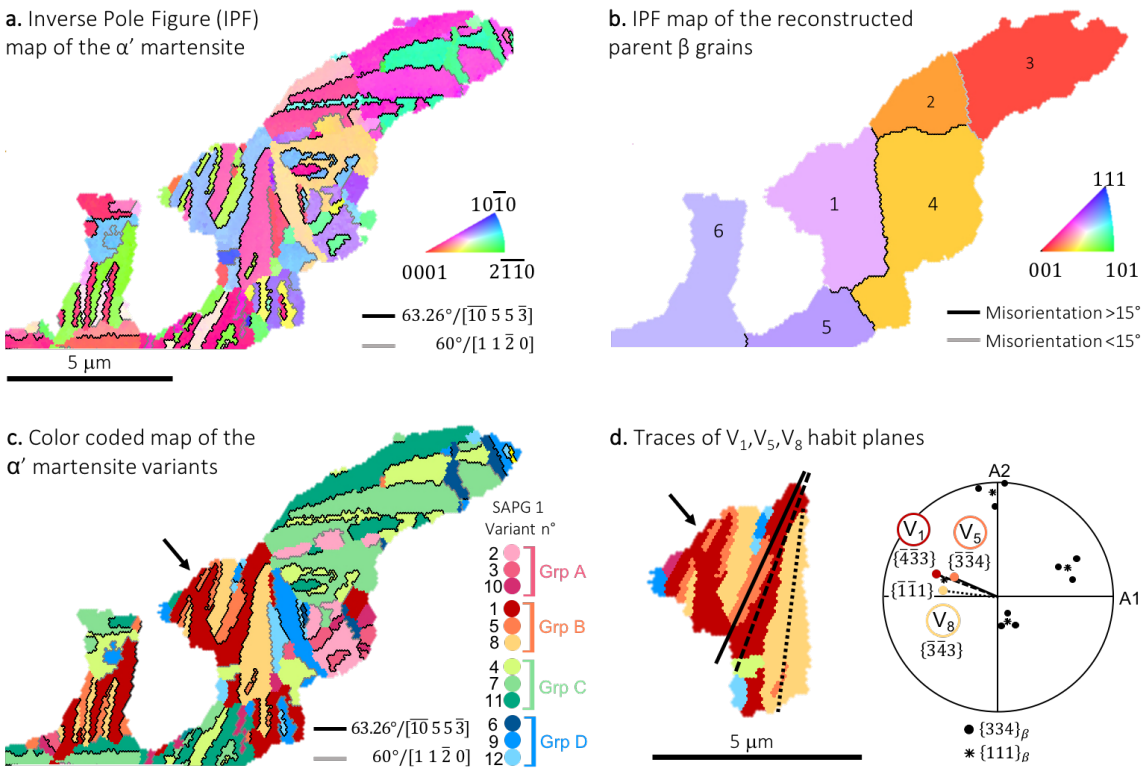

Fig. 3 a : IPF map of the α' martensite, b : IPF map of the reconstructed parent β grains, c : Color coded map of the α' martensite variants, d : $\{\mathbf{334}\}_{\boldsymbol{\beta}}$ pole figure of the HPs of the variants formed in grain 1 and their corresponding traces superimposed onto the map of the variants.

4.1.2. Nature of the intervariant boundary plane associated with a misorientation of $63.26°/[\overline{10}\ 5\ 5\ \bar{3}]_{\alpha'}$

TEM observations were performed to identify the nature of the interface between two adjacent variants of a SAPG 1. Fig. 4a is a bright field micrograph showing parallel martensite plates. Fig. 4b is the Selected Area Diffraction Pattern (SADP) taken from the area encircled in red in Fig. 4a. This area covers two variants as well as their interface. This SADP actually consists of two patterns of the $\langle 1\bar{2}13\rangle_{\alpha'}$ zone axis related by a rotation of 180° about the normal to the $(13\bar{4}1)_{\alpha'}$ plane presented in Fig. 4c and d. The projected trace of this plane is parallel to the projected trace of the interface between the two plates (see Fig. 4a and b). Hence, the two plates are twin-related, and their interface plane correspond to the $(13\bar{4}1)_{\alpha'}$ twinning plane. Individual SADP of the variants on either side of the interface were indexed using ASTAR software. This enabled their absolute orientations to be determined. The following Euler angles (in Bunge notation) were obtained for the matrix and twin orientations: $[192\ 32\ 329]_{(M)} = [224\ 149\ 150]_{(T)}$. The misorientation between these two orientations is calculated to be only 0.66° away from the ideal misorientation of 63.26° expected between the variants of a SAPG 1 [25]. All these elements show that variants pertaining to the same SAPG 1 are twin related with each other and that the associated twinning plane is $\{13\bar{4}1\}_{\alpha'}$. To the author's knowledge, the experimental observation of such a twinning plane has never been reported in the literature so far. The exact nature of this twinning plane will be discussed in more details later. As mentioned above, Beladi et al. [30] estimated this interface plane to be $(4\bar{1}\bar{3}0)_{\alpha'}$ using a stereological procedure. This estimation is about 8.6° away from the exact $\{13\bar{4}1\}_{\alpha'}$ twinning plane identified in the present study.

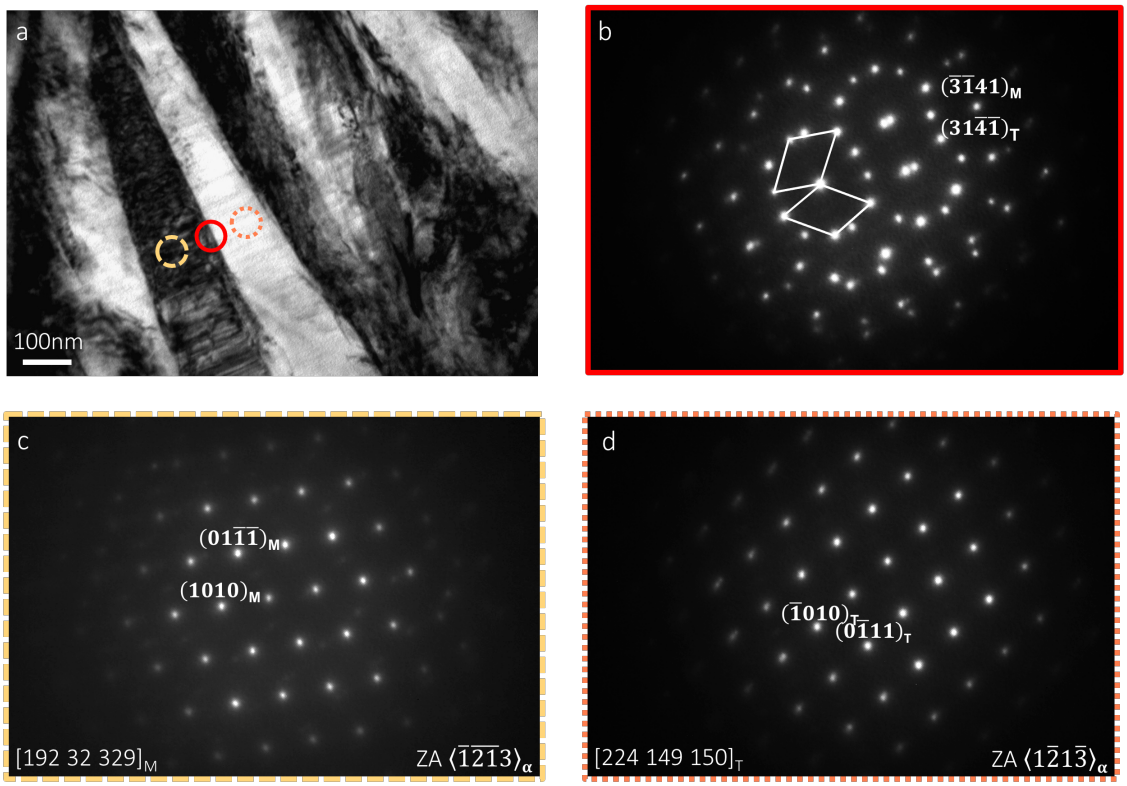

Fig. 4 a : Bright field micrograph of 2 parallel martensite plates, b : SAED pattern of the area encircled in red in Fig. 4a , c : SAED pattern of the area encircled in yellow (lath in dark of the left on the studied interface) in Fig. 4a, d : SAED pattern of the area encircled in orange (bright lath on the right on the studied interface) in Fig. 4a.

The identification of the intervariant boundary plane is further confirmed by a trace analysis on the EBSD map of the grain 2 of Fig. 3 presented in Fig. 5. The traces of the $\{13\bar{4}1\}_{\alpha'}$ interface planes between the variants of the same SPAG 1 formed in grain 2 of Fig. 3 in the stereogram (Fig. 5b) are parallel to the traces of the interfaces between the variants in the IPF map of this grain (Fig. 5a). Each pair of the three variants in the same SAPG 1 formed in grain 2 are related by a rotation of 180° around the normal of the $\{13\bar{4}1\}_{\alpha'}$ interface plane. In order to confirm that the same twinning relationship is found between each pair of the three variants in all the SAPG 1s, these observations has been checked on several different SAPG 1s. The stereographic projection of Fig. 5b reveals

another unexpected feature about the nature of the interface between the variants of the same SAPG 1. Indeed, it appears that each $\{13\bar{4}1\}_{\alpha'}$intervariant boundary plane in a SAPG 1 is strictly parallel to a $\{332\}_{\beta}$ plane which is best known as the specific twinning plane of β metastable alloys [32]. This observation has been checked on several different SAPG 1s. The significance of this observation will be discussed in more details later.

In this first part, the crystallography of the α' martensite of the dual-phase microstructure has been exhaustively studied. The following part aims at investigating its behavior under an applied stress during plastic straining.

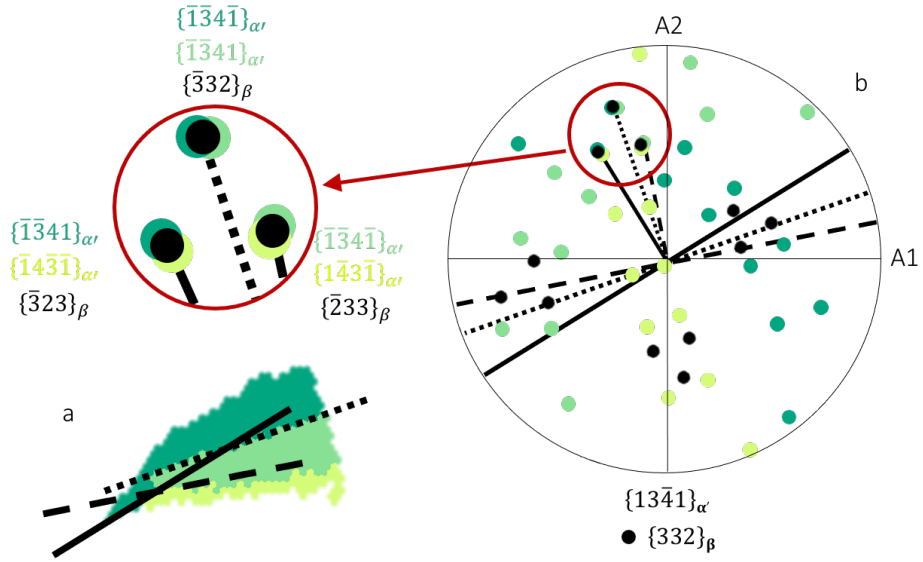

Fig. 5 a : IPF map of the variants formed in grain 2 of Fig. 3. ; b : $\{\mathbf{13\bar{4}1}\}_{\alpha'}$ stereographic projections of the 12 possible variants that could form in grain 2 superimposed onto the $\{\mathbf{332}\}_{\boldsymbol{\beta}}$ pole figure of the parent β grain.

4.2. *Effect of plastic deformation on the α' self-accommodated structure*

Fig. 6a is the IPF map of the α' martensite of the Ti-6Al-4V dual-phase microstructure after 7% of uniform deformation under uniaxial tension. The tensile direction is orthogonal to the plane of the image. The two particular misorientations 63.26°/

$[\overline{1}0\ 5\ 5\ \overline{3}]_{\alpha'}$ and $60°/[1\ 1\ \overline{2}\ 0]_{\alpha'}$ between α' martensite plates are still depicted by dark and grey lines respectively. In some grains, (like n°1, 2, 3 and 4), the fraction corresponding to $63.26°/[\overline{1}0\ 5\ 5\ \overline{3}]_{\alpha'}$ misorientation has been greatly decreased. More precisely, considering all the grains in the IPF map, the fraction of the one at $60°/[1\ 1\ \overline{2}\ 0]_{\alpha'}$ has remained nearly unchanged (0.16) under an applied stress during plastic deformation whereas the one at $63.26°/[\overline{1}0\ 5\ 5\ \overline{3}]_{\alpha'}$ has been greatly decreased to 0.05.

Fig. 6b is the color-coded map of the α' martensite variants corresponding to Fig. 6a. Comparison with Fig. 3c shows that the microstructure has significantly changed during deformation. More precisely, after deformation, the variants of many prior β grain are not present in equal proportions and do not display well-defined plate shape. Two extreme cases are present. In one instance, a single variant remains in a prior β grain after deformation (see grains 1, 2, 3 and 4 in Fig. 6b). In the other case, the variants in a prior β grain are still present in almost equal proportions and display well-defined plate shapes after deformation (see grain 8 in Fig. 6b). In both cases, parent β grains are not composed anymore of complete SAPG 1s composed of 3 variants after deformation. This suggests that the interface related to the $63.26°/[\overline{1}0\ 5\ 5\ \overline{3}]_{\alpha'}$ misorientation is mobile under deformation and that particular variants can grow at the expense of others. Such a specific deformation mechanism is known as *variant reorientation*[1] and is usually a prerogative of the martensite formed in shape memory alloys [33]. In order to assess whether the martensite formed in the present alloy is capable of such a reorientation, it is proposed to

[1] It is important to stress that reorientation does not actually mean that a specific variant undergoes a change in its crystallographic orientation. It rather grows at the expense of the other variants of the same group. This preferential growth leads to a reorientation at the scale of the group of the growing variant.

quantify the work done by the shape deformation associated with the formation of each variant in the direction of the applied stress. In other words, this work corresponds to the interaction of the stress with the shape deformation. This work is referred to as the Interaction Energy (IE) in the literature. More precisely, reoriented variants are expected to maximize this energy. The IE of a particular variant Vi is calculated to be [27]:

$$IE_{Vi} = Trace(\sigma * S_{Vi}^{T}) \quad \textbf{Eq. 2}$$

IE_{Vi} and S_{Vi} are the interaction energy and the shape strain of variant Vi, respectively and σ the macroscopic stress tensor, which in the present case is a simple uniaxial tension along the z-axis.

Fig. 6c shows the IE map of two grains, each representing one of the two extreme cases (grain 1 and 8). IE values are represented using a color gradient from blue for the lowest to red for the highest. Each IE map comes along with a table gathering the IE of the 12 variants that could form from the associated parent β grain as well as the surface fractions of the variants that are actually formed. Furthermore, the IPF of the tensile direction of each parent β grain is given.

In the case of a complete reorientation (see prior β grain 1 in Fig. 6), variant V_9 which has the highest surface fraction in the deformed sample, displays also the highest IE. Its corresponding IE map accordingly appears totally red. The two other variants that belong to the same SAPG 1D, namely variants V_6 and V_{12}, have negative IEs. Therefore, this SAPG 1 is composed of one favorably oriented variant that is growing upon deformation at the expense of two unfavorably oriented variants to accommodate the external stress, leading to a reorientation at the scale of the SAPG 1. In this case, the IPF of the tensile

direction (see Fig. 6c) shows that the direction of the prior β grain which is parallel to the loading direction is very close to the $\langle 101 \rangle_\beta$ direction.

In grain 8 in Fig. 6, the variants exhibit roughly equal surface fractions and present well-defined plate shapes after deformation. Variants from the four different SAPG 1s (A, B, C, D) are present in this grain. It can be checked that these three groups have in common to be composed of two favored variants (positive IE) and one unfavored (negative IE) and that the unfavored variant is not present after deformation. Therefore, this SAPG 1 is composed of two favorably oriented variants that grow upon deformation at the expense of the unfavorably oriented variant. All this suggests that reorientation occurs at the scale of two variants of the same SAPG 1 by the motion of the interface corresponding to misorientation of 63.26° when one variant is favored and the other is unfavored. In grain 8, only few couples of variants in their respective SAPG 1s respect this condition leading to a small volume reoriented. In this case, the normal direction of the prior β grain orientation which is parallel to the loading direction is very close to the $\langle 100 \rangle_\beta$ direction (see Fig. 6c).

Fig. 6b shows that grains n°5, 6 or 7 are partially reoriented. Grain 5 is a typical example of this intermediate case. A detailed analysis of its IE and variant surface fractions is given in Appendix A. 3. This grain is transformed into several SAPG 1s that are each made up of one favored variant and two unfavored. Though a similar configuration led to a complete reorientation in the case of grain 1, a significant surface fraction of unfavored variants remains after deformation in this grain. Nevertheless, the variants with the largest surface fractions are still in that case those with high IE. In this case, the direction of the

prior β grain which is parallel to the loading direction is not so far from the $\langle 101 \rangle_{\beta}$ direction (see Appendix A. 3). This scenario will be further studied later on.

It can be stressed that the present analysis has been carried out on a total of 16 parent β grains with different reorientation scenarios: 7 completely reoriented, 6 partially reoriented and 3 that do not seem to be reoriented.

In summary, it was demonstrated that a reorientation process takes place between the variants of a same SAPG 1 in the α' martensite of the dual-phase microstructure under uniaxial tension. For the reorientation to be effective between two variants, one has to be favored (positive IE) and the other unfavored (negative IE). In that case, the favored variant grows at the expense of the other. Consequently, for the reorientation to be complete in the volume of a SAPG 1, it seems necessary for the SAPG 1 to be made up of one favored variant and two unfavored. This reorientation is thought to occur by the motion of the $\{13\bar{4}1\}_{\alpha'}$ twin boundaries between the variants of the same SAPG 1 which suggests detwinning of thermal martensite.

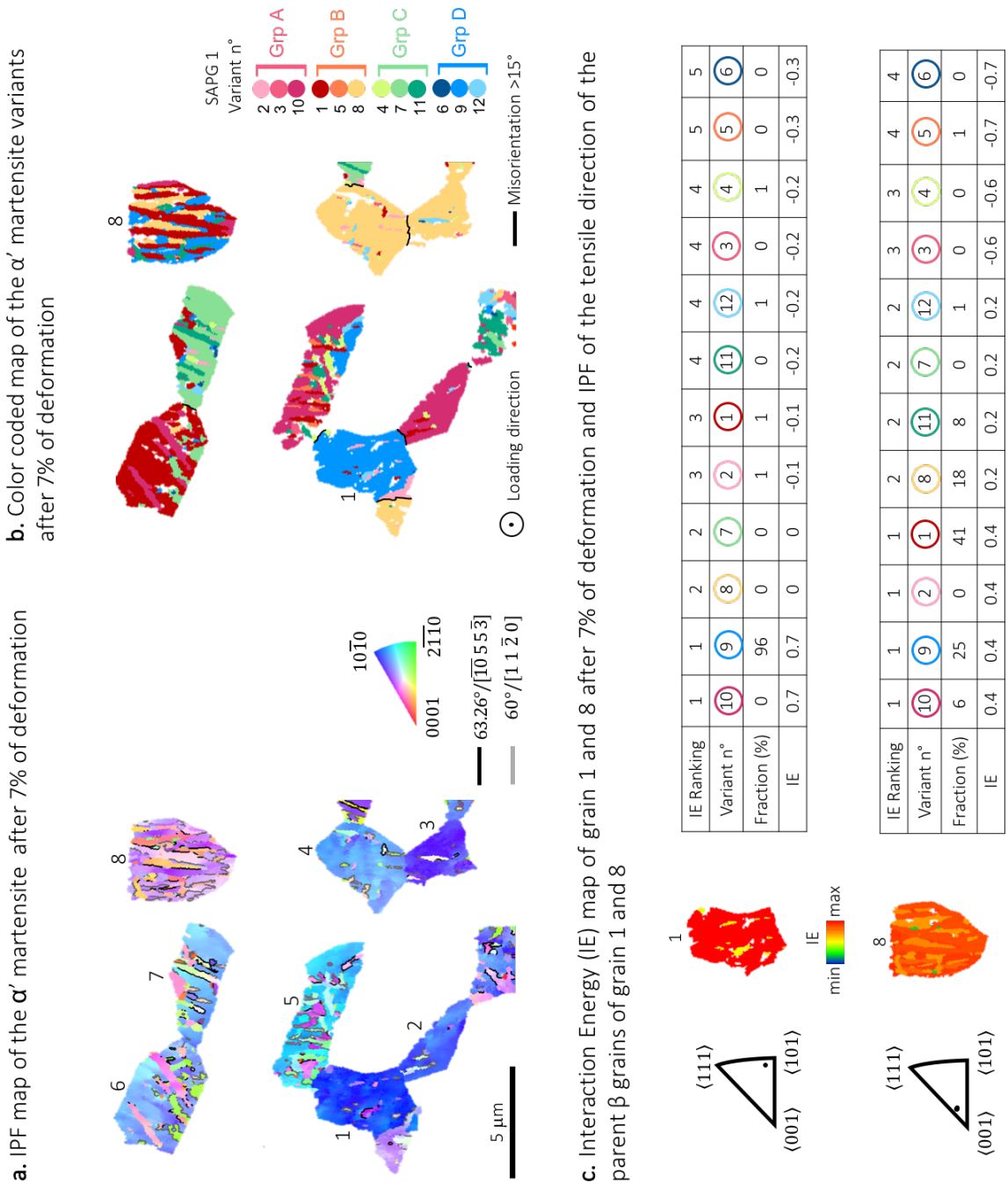

IE Ranking	1	1	2	2	3	3	4	4	4	4	5	5
Variant n°	10	9	8	7	2	1	11	12	3	4	5	6
Fraction (%)	0	96	0	0	1	1	0	1	0	1	0	0
IE	0.7	0.7	0	0	-0.1	-0.1	-0.2	-0.2	-0.2	-0.2	-0.3	-0.3

IE Ranking	1	1	1	1	2	2	2	2	2	3	3	4	4
Variant n°	10	9	2	1	8	11	7	12	3	4	5	6	
Fraction (%)	6	25	0	41	18	8	0	1	0	0	1	0	
IE	0.4	0.4	0.4	0.4	0.2	0.2	0.2	0.2	-0.6	-0.6	-0.7	-0.7	

Fig. 6 a : IPF map of α' martensite after 7% of deformation, b : Color-coded map of the reconstructed variants, c : IE of 12 possible variants of the transformation and their respective experimental surface fractions. IPF of the tensile direction in the parent β grain and color-coded IE map.

5. Discussion

5.1. *Crystallography of the α' martensite of the Ti-6Al-4V dual-phase microstructure*

5.1.1. Morphology of the α' martensite

The studies reported so far on titanium α' martensite mainly concern the as-quenched phase, obtained when formed from the β-phase field [30]. In this case, the martensite is single-phase with a higher content of aluminum (wt%) and a lower content of vanadium (i.e. Ti-6Al-4V nominal composition) compared to the martensite of dual-phase microstructure composed of 4.5wt% of aluminum and 6.8wt% of vanadium. It is well known that during the annealing in the β field, β grains grow very rapidly to reach an average grain size about 500μm [30]. Hence, previous studies have focused on martensite formed in quite large β grains, and in such a case, the β to α' phase transformation occurs through a sequential fragmentation process [19]. The first variants to form are large martensite plates that conforms to the constraining effect of the parent β matrix. Therefore, among all the 12 variants that could form from the parent β grain, there is a priori no reason for one variant to be favored among the others as the constraining effect of the parent β grain is the same for each variant. At this stage of the transformation, it is believed that all 12 variants are equiprobable. However, once a first variant is formed, the shape deformation associated with this transformation creates such a stress field around this variant that only a few other variants can form in its vicinity so as to minimize the overall deformation of the β grain. The next generations of plate form within the remaining spaces left untransformed by the plates of the previous generations. At each generation, the size of the transforming plates decreases in accordance with the

progressive reduction of the available space in the parent phase. In that case, coarse variants and fine variants are distinguishable. This progressive reduction of the transformable volume significantly constrains the martensitic transformation and increases the need for the martensite plate to mutually compensate for their shape strains. In the present study, the α' martensite of the dual-phase microstructure is obtained through a quench from the sub-transus α+β field. During the annealing in the α+β field, β grains growth is impeded by the pre-existing equiaxed α grains and their average grain size remains below 10μm. This grain size scales roughly with the size of the last pockets that transform when the transformation occurs sequentially (see Fig. 1). Indeed, perpendicular and V-shape couplings of variant are much less frequent. Rather, all the martensite plates that form in one grain share the same characteristic length scale and are stacked in a parallel way (see Fig. 3). A similar configuration of parallel plates has been observed in precipitates of tetragonal zirconium surrounded by an untransformable material [34]. In that case, such parallel configurations were thought to result from the need of self-accommodation between the martensite plates that is required by the constraining effect of the untransformable environment. A similar explanation can be given in our case if one considers that in the dual-phase microstructure the prior β grains are surrounded by α grains that do not transform during quenching. These α grains should similarly constrain the phase transformation that takes place in the small β grains and explain the preferential formation of self-accommodating plate group of type I (SAPG 1) in the dual-phase microstructure (see Fig. 3).

5.1.2. Self-accommodating plate groups

EBSD analysis confirmed that the martensite plates formed in the dual-phase microstructure are mostly cluster of type 1 self-accommodating plate groups of variants (SAPG 1). The characteristic parallel morphology of SAPG 1 is explained by the observation that the habit planes of the three variants of the same SAPG 1 are almost parallel to each other and close to a common $\{111\}_{\beta}$ plane. Various authors have predicted theoretically that the SAPG 1 configuration offers the best possible accommodation among all the possible SAPGs that could form during the β to α' transformation [25][31]. Despite this prediction, to the author's knowledge, SAPG1s had never been observed experimentally before the present study. To date, indeed, the configuration of SAPG 2 is, by far, the most commonly reported in the cases of the β-α' and β-α'' (orthorhombic martensite) transformations [30-31] . In such a configuration, it can be checked that the HPs of the variants of the same SAPG 2 are at around 62° from each other which is consistent with the martensite plates of a SAPG 2 organizing themselves in a triangular manner [31]. The fact that the SAPG 1 configuration is favored over the SAPG 2 in the present case may hardly be related to the minor difference in their relative degree of self-accommodation [25]. Another possible explanation may be related to the nature of the intervariant boundary interface associated with each configuration and more specifically to the surface energy associated with these two particular interfaces. Previous studies showed that the variants of the same SAPG 2 (misorientation of 60°) are twin related on $\{10\bar{1}1\}_{\alpha'}$ type planes. Beladi et al. [30] confirmed that this twinning plane corresponds to the intervariant boundary plane between variants separated by a misorientation at 60° in a Ti-6Al-4V alloy. As stated out by Srivastava et al. [31], these $\{10\bar{1}1\}_{\alpha'}$ type twin planes derive from $\{110\}_{\beta}$ mirror plane in the parent β phase and are

therefore thought to be favorable, form surface energy considerations. Based on molecular dynamic simulations, Beladi et al. [30] confirmed that the twinning plane is the low energy one and thereby, it is expected that this plane should be experimentally favored among the others possible intervariant planes. Yet, in our case, this $\{10\bar{1}1\}_{\alpha'}$ interface, which could only be observed in between two priors β grains or in between two SAPG 1s is much less favored than that between the variant of a same SAPG 1. Rather, TEM analysis clearly showed for the first time that the variants of the same SAPG 1 (misorientation of 63.26°) are also twin related but, in this case, on $\{13\bar{4}1\}_{\alpha'}$ type twinning planes. Interestingly, the $\{13\bar{4}1\}_{\alpha'}$ twinning plane corresponds to the K_1 plane of one of the possible twinning modes in titanium that have been predicted by the theory of Bevis and Crocker [26]. However, these authors emphasized that the twinning mode associated with this $\{13\bar{4}1\}_{\alpha'}$ twinning plane was not expected to occur experimentally, based on the fact that, among its four twinning elements, only η_1 was irrational. Noteworthy, similarly to the $\{10\bar{1}1\}_{\alpha'}$ twinning plane, the $\{13\bar{4}1\}_{\alpha'}$ twinning plane is also associated to a particular β plane. The stereographic analysis in Fig. 5 shows that each $\{13\bar{4}1\}_{\alpha'}$ interface plane is indeed strictly parallel to a $\{332\}_{\beta}$ plane of the parent β grain which is best known as the specific twinning plane of β metastable alloys [32]. Interestingly, Bertrand et al. [32] identified a similar correspondence between the twinning elements of the $\{130\}\langle 310\rangle_{\alpha''}$ mechanical twinning system of α'' orthorhombic martensite and that of the $\{332\}\langle 11\bar{3}\rangle_{\beta}$ mechanical twinning system of the parent bcc β phase in Ti-25Ta-20Nb shape memory alloy. Though it is rather difficult at this point to derive all the consequences of these correspondences, they both lead to the need of a better understanding related to the link between the $\{332\}\langle 11\bar{3}\rangle_{\beta}$ twinning system and the martensitic transformation in Ti alloys.

5.2. *Reorientation of the variants of the α' martensite on the Ti-6Al-4V dual-phase microstructure under the effect of deformation*

5.2.1. Rationalization and prediction of reorientation

Another remarkable property of the $\{13\bar{4}1\}_{\alpha'}$ interface plane that has been indirectly evidenced for the first time in the present study is that it is mobile under deformation. This was experimentally assessed based on the sharp decrease in the number of its associated misorientations at 63.26° in the IPF map after 7% of uniform deformation and on the observation that particular variants grow at the expense of some others in the variant reconstruction map (see Fig. 3a and c). By contrast, the misorientation at 60° remains to its starting low proportion after deformation, which suggests that this interface is not mobile under deformation. Therefore, the reorientation phenomenon that takes place in the α' martensite of the dual-phase microstructure is only due to the movement of the $\{13\bar{4}1\}_{\alpha'}$ interface. Such a specific deformation mode is generally thought to only occur in shape-memory alloys, including the titanium-based alloys that are highly enriched in β-stabilizing alloying elements such as Ti-Nb [34–37] or Ti-Ta-Nb [32] and transforming into orthorhombic α'' martensite. In our case, hcp α' martensite is also enriched in one β-stabilizing elements, namely vanadium. Previous studies [38] showed that its enrichment is about 6.5wt% of V content which is not enough to bring a change in the crystallographic structure from the hexagonal closed-packed α' martensite to the orthorhombic α'' martensite (the critical enrichment is about 10wt% [15]). However, similarly to Tobe et al. [39], this low enrichment in β-stabilizing alloying element may be sufficient to lower the magnitude of the twinning shear associated with the movement of the $\{13\bar{4}1\}_{\alpha'}$ interface. This could lead to a lower required stress to induce deformation

via the movement of this twinning plane and hence to the reorientation of the martensite of the dual-phase microstructure. In shape memory alloys, the usual method to predict reorientation differs from the one proposed here. More precisely, it consists in the determination of which Correspondence Variant (CV) maximizes the strain along the tensile direction instead of the determination of the one whose growth maximizes the work along the tensile direction (maximum IE). The former method is based on the calculation of the lattice deformation that is generated by the formation of each CV [32]. In contrast, in the present work, similarly to what is classically done in TRIP steels [27], the calculation is based on the shape strain associated with each variant. Beside the Bain deformation, the shape strain also includes a rotation and a LIS and constitutes therefore a more realistic description of the total deformation associated with the transformation. The reorientation predictions only based on the lattice deformation are reported in Appendix A. 4 and the description of the calculation are given in Appendix A. 5. As expected, comparison between Fig. 6c and Appendix A. 4. shows that both methods predict the same tendencies. The variants that are growing maximize the strain along the tensile direction. However, none of these two criterions (maximum IE or maximum strain along the tensile direction) is sufficient on its own to completely explain the growth of the variant considered. As shown in Fig. 6c, for the reorientation to be effective between two variants, one variant has to be favored (positive IE) and the other unfavored (negative IE). In that case, the favored variant can grow at the expense of the other and this reorientation is thought to occur by the motion of the $\{13\bar{4}1\}_{\alpha'}$ twin boundaries between the variants of the same SAPG 1. Therefore, for the reorientation to be complete in the volume covered by a SAPG 1, the favored variant (positive IE) has indeed to be accompanied in its SAPG 1 by two unfavored variants (negative IE) (see grain 1 in Fig.

6b). For this purpose, as soon as there are two favored variants of a SAPG 1, they can only grow in the volume covered by the unfavored variant which is indeed not present after deformation (see grain 8 in Fig. 6b). This suggests that, in that case, the tendency of each favored variant to grow at the expense of the other mutually compensate, thereby leaving the interface immobile between these variants. It has to be kept in mind that some parent β grains may transform into several SAPG 1s. In the SAPG 1s that respect the criterion to induce a *complete* reorientation, the favored variant will grow only in the volume covered by its own group. Its growth will indeed be stopped at the interface with its neighboring SAPG 1 (this case corresponds to grains 5, 6 and 7 in Fig. 6). After deformation, such grains are composed of at least as many variants as the number of SAPG1s and appear therefore partially reoriented.

5.2.2. Effect of texture on reorientation

The reorientation criterion of a specific SAPG 1 is closely related to the orientation of the parent β grain with respect to the loading direction. Experimentally, grain 1 and grain 8 showed two very distinct behaviors depending on the orientation of the prior β grain with respect to the macroscopic tensile direction. In the case of a complete reorientation (grain 1), the direction of the prior β grain which is parallel to the loading direction is very close to the $\langle 101 \rangle_\beta$ direction whereas, in the case of SAPG 1s composed of several favored variants (grain 8), the direction of the prior β grain which is parallel to the loading direction is very close to the $\langle 100 \rangle_\beta$ direction (see Fig. 6c). These results show that the reorientation critically depends on the loading direction. To get better insights into this dependency, a theoretical study was carried out. A set of 5000 random orientations of the parent β phase was generated. For each β orientation, the crystal direction parallel to the

loading direction is determined and the number of SAPG 1s of this β orientation that can induce a complete reorientation in the volume covered by the group, i.e. consisting of one favored variant and two unfavored variants is calculated. The results are plotted as a color coded IPF in Fig. 7, with the loading direction as a reference. There are four possible cases ranging from a minimum of zero to a maximum of three groups that meet the criterion among the four SAPG 1s. For a tensile direction within 25° of $\langle 100 \rangle_\beta$, there is no SAPG 1 that fulfils the criterion to induce a complete reorientation. These orientations appear in grey in Fig. 7. Grain 8 in Fig. 6 corresponds to this particular case. As shown in Fig. 6c, the four SAPG 1s that could form from the parent β grain that is associated to grain 8 are indeed all composed of more than one variant which is favored. For all the other loading conditions, there is at least one SAPG 1 that fulfils the criterion to induce a complete reorientation. More precisely, two SAPG 1s fulfill the criterion when the loading direction is close to $\langle 101 \rangle_\beta$ (orange in Fig. 7). Grain 1 in Fig. 6 corresponds to this particular case. As shown in Fig. 6c, there are two SAPG 1s among the four that could form from the parent β grain associated to grain 1 that are indeed composed of one variant which is favored and two that are unfavored. Three SAPG 1s fulfill the criterion when the loading direction is close to $\langle 111 \rangle_\beta$ (red in Fig. 7) respectively. For the remaining loading directions, only one SAPG 1 fulfills the criterion.

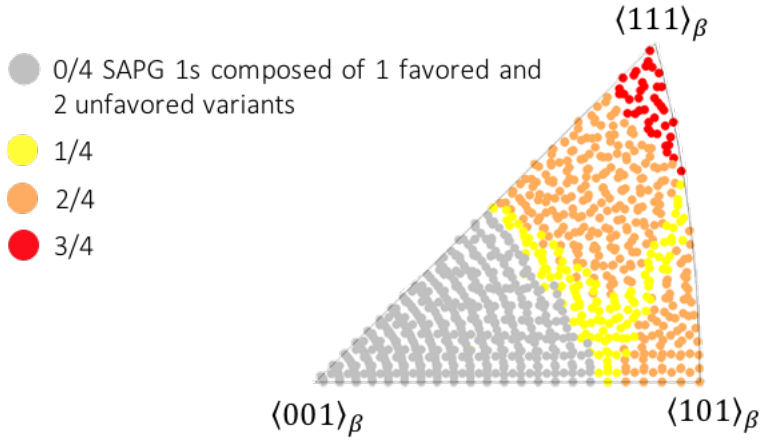

Fig. 7 Color coded IPF of the tensile direction in the parent β grain showing the number of SAPG 1s that are composed of a favored variant and two unfavored variants (grey=0, yellow=1, orange=2 and red=3)

This evidence the dramatic influence of the parent β phase on the reorientation. In the present study, the forging process is believed to induce a preferential $\langle 101\rangle_\beta$ α fiber texture, which is favorable to induce complete reorientation [40]. This explains why it has been possible to observe many reoriented variant groups after deformation. The probability to induce a complete reorientation for the $\langle 111\rangle_\beta$ oriented grains is higher than that of the $\langle 101\rangle_\beta$ grains (3 groups from 4 can completely reorientate, in that case). However, the Interaction Energy (IE) associated with growth of the variants is not the same for both cases since it depends on the tensile direction. In order to quantify this dependency, a theoretical study is carried out on the same set of grains as in Fig. 7. For each β orientation, the maximum IE of the 12 possible variants is calculated. The results are plotted as a color coded IPF of the loading direction in Fig. 8. The maximum IE is obtained for $\langle 101\rangle_\beta$ grains whereas the minimum corresponds to the $\langle 111\rangle_\beta$ grains.

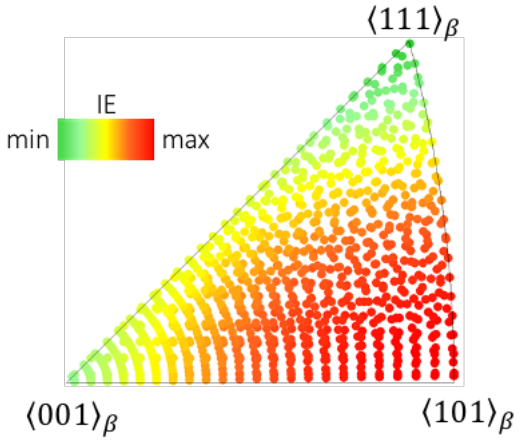

Fig. 8 Color coded IPF of the tensile direction in the parent β grain showing the maximum values of IE of the 12 possible variants

As mentioned above, this IE is directly correlated with the lattice deformation of the variants which is better suited to quantify the strain associated to the growth of specific martensitic variants. Similar to Fig. 8, for each β orientation, the maximum lattice deformation of the 12 possible variants is calculated and the results are plotted as a color coded IPF of the loading direction in Fig. 9. The highest possible lattice deformation among the 12 variants that could form in each grain of Fig. 6 (from n°1 to n°8) is highlighted in Fig. 9. As expected, the maximum and minimum lattice deformations are obtained for $\langle 101 \rangle_\beta$ and $\langle 111 \rangle_\beta$ grains respectively. Hence, although $\langle 111 \rangle_\beta$ grains have the highest probability to induce complete reorientation (see Fig. 7.), they will poorly accommodate the stress (low strain along the tensile direction). By contrast, $\langle 101 \rangle_\beta$ grains correspond to a better compromise since they have a relatively high probability to induce complete reorientation and are very efficient to accommodate large strain along the tensile direction.

The maximum lattice deformation which is obtained in the most favorable case of $\langle 101 \rangle_\beta$ oriented grains is around 9%.

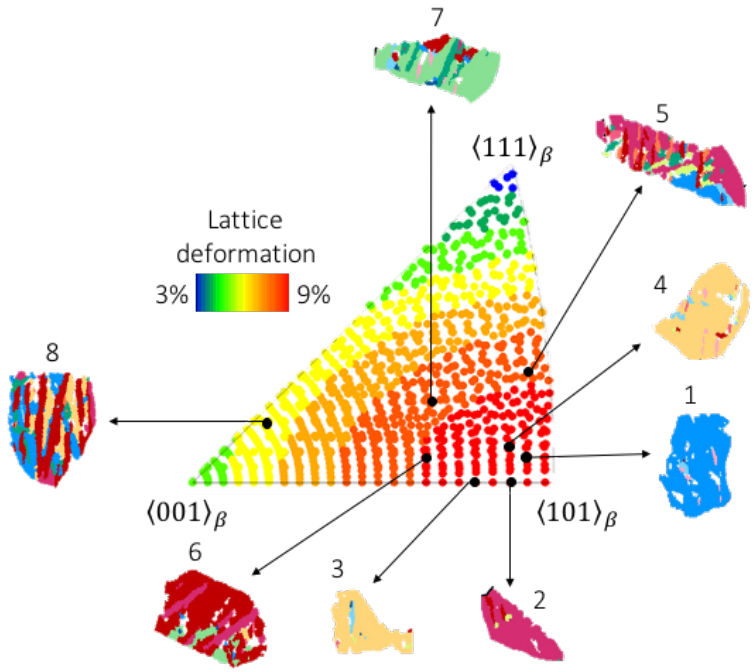

Fig. 9 IPF of the tensile direction in the parent β grain showing the maximum values of lattice deformation of the 12 possible variants

Interestingly, this value is twice as large as the maximum lattice deformation that can be reached by the reorientation of α'' orthorhombic martensite in Ti-Nb shape memory alloys. This stems from the fact that in our case, the β to α' (hcp) martensitic transformation is associated with a larger lattice deformation. As a consequence, the reorientation mechanism brings a large amount of ductility to the α' martensite of the dual-phase microstructure in the parent β grains that have a $\langle 101 \rangle_\beta$ texture. By contrast, the α' titanium martensite has generally a poor ductility that relies only on dislocation glide. In the α' martensite of the dual-phase microstructure, the reorientation is an additional deformation mechanism that acts in combination with dislocation glide to

improve its ductility. The association of this very ductile α' martensite with the hard α phase generates a strong mechanical contrast which is believed to be at the origin of the high work-hardening of the dual-phase microstructure.

6. Conclusions

The V-rich and Al-poor hcp α' martensite formed in Ti-6Al-4V dual-phase microstructure can reorient under uniaxial tension, a property rather usually associated to the orthorhombic α'' martensite in β-Ti alloys and more generally in shape memory alloys. This unexpected deformation mechanism of hcp martensite occurs via the movement of a unique intervariant interface associated with the specific misorientation of $63.26°/[\overline{10}\ 5\ 5\ \bar{3}]_{\alpha'}$. This interface is a hitherto unobserved $\{13\bar{4}1\}_{\alpha'}$ type twin plane which is directly related to the $\{332\}_{\beta}$ specific twinning plane of the parent β phase. Hence, the formation of self-accommodating plate groups of variants misoriented by $63.26°/[\overline{10}\ 5\ 5\ \bar{3}]_{\alpha'}$ is crucial for the occurrence of the reorientation phenomenon. In the present dual-phase microstructure, the preferential formation of this specific kind of SAPG is believed to stem at least partially from the constraining effect of the "untransformable" α phase on the martensite during its formation. Furthermore, a detailed crystallographic analysis allowed to derive a necessary condition for a variant to grow at the expense of another under an external loading. It has to exhibit a positive interaction energy while the other one has to exhibit a negative one. Consequently, for the reorientation to be complete in the volume of a SAPG 1, it seems necessary for the SAPG 1 to be made up of one favored (positive IE) variant and two unfavored (negative IE). In turn, the fulfillment of this criterion to induce a complete reorientation in the volume of a SAPG 1 was shown to depend on the relative orientation of the parent β grain with

respect to the tensile direction. This explains why $\langle 110 \rangle_\beta$ grains are more prone to reorientation than $\langle 100 \rangle_\beta$ grains. Theoretical calculations further predict that reorientation is highly probable can also occur in $\langle 111 \rangle_\beta$ grains. More generally, the reorientation mechanism contributes to the remarkable ductility of the dual-phase microstructure and shed new lights into the microscale deformation of the martensite phase in this newly developed dual-phase microstructure in the well-known Ti-6Al-4V alloy. Further investigations include the determination of the critical resolved shear stress of the reorientation and the observation of the possible reversibility of the mechanism upon heating.

Acknowledgements

The authors are grateful to the F.N.RS, Belgium. for financing this research. The authors wish to acknowledge Benjamin Hary who contributes to this work within the framework of the project Feder IAWATHA. The authors are grateful to Yvon Millet and Timet Savoie for providing the material and for sharing continuous fruitful discussions.

Bibliography

[1] C. Leyens et M. Peters, Éd., *Titanium and Titanium Alloys: Fundamentals and Applications*. Weinheim, FRG: Wiley-VCH Verlag GmbH & Co. KGaA, 2003.

[2] R. K. Gupta, C. Mathew, et P. Ramkumar, « Strain Hardening in Aerospace Alloys », *Front. Aerosp. Eng.*, vol. 4, nº 1, p. 1-13, 2015, doi: 10.12783/fae.2015.0401.01.

[3] G. Lütjering, J.C. Williams, *Titanium*, 2nd ed. Engineering Materials and Processes, 2007.

[4] F. Sun *et al.*, « A new titanium alloy with a combination of high strength, high

strain hardening and improved ductility », *Scr. Mater.*, vol. 94, p. 17-20, janv. 2015, doi: 10.1016/j.scriptamat.2014.09.005.

[5] F. Sun *et al.*, « Strengthening strategy for a ductile metastable β -titanium alloy using low-temperature aging », *Mater. Res. Lett.*, vol. 5, nº 8, p. 547-553, nov. 2017, doi: 10.1080/21663831.2017.1350211.

[6] C. Brozek *et al.*, « A β-titanium alloy with extra high strain-hardening rate: Design and mechanical properties », *Scr. Mater.*, vol. 114, p. 60-64, mars 2016, doi: 10.1016/j.scriptamat.2015.11.020.

[7] C. de Formanoir *et al.*, « A strategy to improve the work-hardening behavior of Ti–6Al–4V parts produced by additive manufacturing », *Mater. Res. Lett.*, p. 1-8, oct. 2016, doi: 10.1080/21663831.2016.1245681.

[8] C. de Formanoir *et al.*, « Micromechanical behavior and thermal stability of a dual-phase α+α' titanium alloy produced by additive manufacturing », *Acta Mater.*, vol. 162, p. 149-162, janv. 2019, doi: 10.1016/j.actamat.2018.09.050.

[9] Y. Chong, G. Deng, J. Yi, A. Shibata, et N. Tsuji, « On the strain hardening abilities of α+β titanium alloys: The roles of strain partitioning and interface length density », *J. Alloys Compd.*, vol. 811, p. 152040, nov. 2019, doi: 10.1016/j.jallcom.2019.152040.

[10] K. Sofinowski *et al.*, « In situ characterization of a high work hardening Ti-6Al-4V prepared by electron beam melting », *Acta Mater.*, vol. 179, p. 224-236, oct. 2019, doi: 10.1016/j.actamat.2019.08.037.

[11] L. Morsdorf, O. Jeannin, D. Barbier, M. Mitsuhara, D. Raabe, et C. C. Tasan,

« Multiple mechanisms of lath martensite plasticity », *Acta Mater.*, vol. 121, p. 202-214, déc. 2016, doi: 10.1016/j.actamat.2016.09.006.

[12] Y. Mazaheri, A. Kermanpur, et A. Najafizadeh, « Nanoindentation study of ferrite–martensite dual phase steels developed by a new thermomechanical processing », *Mater. Sci. Eng. A*, vol. 639, p. 8-14, juill. 2015, doi: 10.1016/j.msea.2015.04.098.

[13] A. Moridi, A. G. Demir, L. Caprio, A. J. Hart, B. Previtali, et B. M. Colosimo, « Deformation and failure mechanisms of Ti-6Al-4V as built by selective laser melting », *Mater. Sci. Eng. A*, vol. 768, p. 25, 2019, doi: 10.1016/j.msea.2019.138456.

[14] H. Matsumoto, H. Yoneda, D. Fabregue, E. Maire, A. Chiba, et F. Gejima, « Mechanical behaviors of Ti–V–(Al, Sn) alloys with α′ martensite microstructure », *J. Alloys Compd.*, vol. 509, nº 6, p. 2684-2692, févr. 2011, doi: 10.1016/j.jallcom.2010.11.089.

[15] H. M. Flower, R. David, et D. R. F. West, « Martensite formation and decomposition in alloys of titanium containing β-stabilizing elements », in *Titanium and Titanium Alloys Scientific and Technological Aspects Volume 3.*, Springer Verlag, 2014, p. 1703-1715.

[16] R. Castro et L. Séraphin, « Contribution à l'étude métallographique et structurale de l'alliage de titane TA6V », *Mém. Sci. Rev. Métallurgie*, 1966.

[17] J. H. Richardson et R. V. Peterson, *Systemic materials analysis. Volume IV Volume IV*. New York: Academic Press, 1978.

[18] H. Liebowitz, « I : Microscopic and Macroscopic Fundamentals II: Mathematical Fundamentals III : Engineering Fundamentals and Environmental Effects IV:

Engineering Fracture Design V: Fracture Design of Structures VI: Fracture of Metals VII : Fracture of Nonmetals and Composites », p. 513.

[19] S. Banerjee et P. Mukhopadhyay, « Martensitic Transformations », in *Pergamon Materials Series*, vol. 12, Elsevier, 2007, p. 257-376.

[20] « SAE AMS 4928: Titanium Alloy Bars, Wire, Forgings, Rings, and Drawn Shapes 6Al-4V annealed ». SAE International, déc. 07, 2017.

[21] J. K. Mackenzie et J. S. Bowles, « The crystallography of martensite transformations—IV body-centred cubic to orthorhombic transformations », *Acta Metall.*, vol. 5, nº 3, p. 137-149, 1957, doi: https://doi.org/10.1016/0001-6160(57)90018-4.

[22] J. C. Bokros et E. R. Parker, « The mechanism of the martensite burst transformation in Fe-Ni single crystals », *Acta Metall.*, vol. 11, nº 12, p. 1291-1301, déc. 1963, doi: 10.1016/0001-6160(63)90024-5.

[23] X. Gu, T. Furuhara, et W. Zhang, « PTCLab: Free and open-source software for calculating phase transformation crystallography », *Journal of Applied Crystallography*, 2016.

[24] D. Srivastava, S. Banerjee, et S. Ranganathan, « THE CRYSTALLOGRAPHY OF THE BCC TO HCP (ORTHOHEXAGONAL) MARTENSITIC TRANSFORMATION IN DILUTE Zr-Nb ALLOYS: Part I: Lattice Strain and Lattice Invariant Shear », *TRANS INDIAN INST MET*, vol. 57, nº 3, p. 19, 2004.

[25] S. C. Wang, M. Aindow, et M. J. Starink, « Effect of self-accommodation on α/α boundary populations in pure titanium », *Acta Mater.*, vol. 51, nº 9, p. 2485-2503, mai

2003, doi: 10.1016/S1359-6454(03)00035-1.

[26] M. Bevis et A. G. Crocker, « The crystallography of deformation twinning in titanium », in *The Science, Technology and Application of Titanium*, 1st Edition., Pergamon Press, 1970, p. 453-458.

[27] H. K. D. H. Bhadeshia, « Prediction and Exploitation of Transformation Texture », *Solid State Phenom.*, vol. 172-174, p. 13-24, juin 2011, doi: 10.4028/www.scientific.net/SSP.172-174.13.

[28] T. Ahmed et H. J. Rack, « Phase transformations during cooling in ?+? titanium alloys », *Mater. Sci. Eng. A*, vol. 243, nº 1-2, p. 206–211, mars 1998.

[29] V. Tong, S. Joseph, A. K. Ackerman, D. Dye, et T. B. Britton, « Using transmission Kikuchi diffraction to characterise α variants in an α+β titanium alloy: TRANSMISSION KIKUCHI DIFFRACTION OF DUAL PHASE TI ALLOYS », *J. Microsc.*, vol. 267, nº 3, p. 318-329, sept. 2017, doi: 10.1111/jmi.12569.

[30] H. Beladi, Q. Chao, et G. S. Rohrer, « Variant selection and intervariant crystallographic planes distribution in martensite in a Ti–6Al–4V alloy », *Acta Mater.*, vol. 80, p. 478-489, nov. 2014, doi: 10.1016/j.actamat.2014.06.064.

[31] D. Srivastava, K. Madangopal, S. Banerjee, et S. Ranganathan, « Self accommodation morphology of martensite variants in Zr-2.5wt%Nb alloy », *Acta Met. Mater*, vol. 41, nº 12, p. 3445-3454, 1993, doi: 10.1016/0956-7151(93)90224-G.

[32] E. Bertrand, P. Castany, Y. Yang, E. Menou, et T. Gloriant, « Deformation twinning in the full-α″ martensitic Ti–25Ta–20Nb shape memory alloy », *Acta Mater.*, vol. 105, p. 94-103, févr. 2016, doi: 10.1016/j.actamat.2015.12.001.

[33] G. Laplanche, T. Birk, S. Schneider, J. Frenzel, et G. Eggeler, « Effect of temperature and texture on the reorientation of martensite variants in NiTi shape memory alloys », *Acta Mater.*, vol. 127, p. 143-152, avr. 2017, doi: 10.1016/j.actamat.2017.01.023.

[34] P. M. Kelly et L. R. F. Rose, « The martensitic transformation in ceramics - its role in transformation toughening », *Prog. Mater. Sci.*, vol. 47, nº 5, p. 465-557, 2002, doi: 10.1016/S0079-6425(00)00005-0.

[35] T. Inamura, J. I. Kim, H. Y. Kim, H. Hosoda, K. Wakashima, et S. Miyazaki, « Composition dependent crystallography of **α** ″-martensite in Ti–Nb-based β-titanium alloy », *Philos. Mag.*, vol. 87, nº 23, p. 3325-3350, août 2007, doi: 10.1080/14786430601003874.

[36] Y. W. Chai, H. Y. Kim, H. Hosoda, et S. Miyazaki, « Self-accommodation in Ti–Nb shape memory alloys », *Acta Mater.*, vol. 57, nº 14, p. 4054-4064, août 2009, doi: 10.1016/j.actamat.2009.04.051.

[37] H. Tobe, H. Y. Kim, T. Inamura, H. Hosoda, et S. Miyazaki, « Origin of {332} twinning in metastable β-Ti alloys », *Acta Mater.*, vol. 64, p. 345-355, févr. 2014, doi: 10.1016/j.actamat.2013.10.048.

[38] C. de Formanoir, « Post-processing of additively manufactured Ti-6Al-4V: improving the mechanical properties of near-net-shape parts », Doctorat en Sciences de l'Ingénieur et Technologies, Université Libre de Bruxelles, 2017.

[39] H. Tobe, H. Y. Kim, T. Inamura, H. Hosoda, T. H. Nam, et S. Miyazaki, « Effect of Nb content on deformation behavior and shape memory properties of Ti–Nb alloys », *J. Alloys Compd.*, vol. 577, p. S435-S438, nov. 2013, doi: 10.1016/j.jallcom.2012.02.023.

[40] D. G. Leo Prakash, P. Honniball, D. Rugg, P. J. Withers, J. Quinta da Fonseca, et M. Preuss, « The effect of β phase on microstructure and texture evolution during thermomechanical processing of α+β Ti alloy », *Acta Mater.*, vol. 61, nº 9, p. 3200-3213, mai 2013, doi: 10.1016/j.actamat.2013.02.008.

[41] L. Germain, N. Gey, et M. Humbert, « Reliability of reconstructed β-orientation maps in titanium alloys », *Ultramicroscopy*, vol. 107, nº 12, p. 1129-1135, nov. 2007, doi: 10.1016/j.ultramic.2007.01.012.

[42] C. Cayron, B. Artaud, et L. Briottet, « Reconstruction of parent grains from EBSD data », *Mater. Charact.*, vol. 57, nº 4-5, p. 386-401, déc. 2006, doi: 10.1016/j.matchar.2006.03.008.

Appendix A. 1 Prior β grain reconstruction algorithm

The parent β grain reconstruction was performed with an in-house MATLAB® software working with α' grains defined by a tolerance angle of 5°. The proposed algorithm is based on a nucleation and growth principle. The originality of this algorithm is that it takes benefits from the fact that among the 5 possible misorientations (distinct from the identity) that exist between variants of the Burger OR, 3 of them correspond to misorientations between two variants sharing the same parent β orientation. Those specific misorientations are described by the following angle/axis pairs: 60.83°/[$\overline{1.377}$ $\bar{1}$ 2.377 0.359], 63.26°/[$\overline{10}$ 5 5 $\bar{3}$] and 90°/[1 $\overline{2.38}$ 1.38 0]. Incidentally, these misorientations frequently result from the martensitic phase transformation in pure Ti and Ti alloys as already shown in the present study and others [19][25]. Therefore, the existence of at least one of this misorientation in each transformed β grain is highly

probable thereby ensuring a reliable reconstruction of the parent orientation. In the nucleation step, such specific misorientations are systematically searched for among all the possible couples of neighbouring α' grains. Once identified, those couples are turned into β phase and their orientation is changed into their common parent β orientation. In the second step of the algorithm, the regions of reconstructed β grains are allowed to grow at the expense of the adjacent α' grains if the Burgers OR is fulfilled with a tolerance angle which is increased by step of 1° from 1° to 5°. This algorithm proved robust and reliable on various martensitic microstructures formed in pure Ti and Ti alloys. Furthermore, since only misorientations between neighbouring grains are considered, this algorithm is faster than those previously proposed. For comparison, a set of 10 000 grains is reconstructed in 20 minutes on a Intel Core i7 CPU, 16Go RAM PC. [41-42]

Appendix A. 2 PTMC inputs (Lattice correspondences, LIS) and outputs (closest Burgers variant, habit planes, shape strain directions) of the 12 variants obtained during the phase transformation of β to α' – identification of the two Self-Accommodating Plate Groups (SAPG) characterized by their respective $\mathbf{63.26°/[\overline{10}\ 5\ 5\ \overline{3}]}$ and $\mathbf{60°/[1\ 1\ \overline{2}\ 0]}$ misorientations

Correspondence	LIS	Variant	Closest Burgers variant	Habit plane	Shape strain direction	SAPG 1 $63.26°/[\bar{1}0\ 5\ 5\ \bar{3}]$	SAPG 2 $60°/[1\ 1\ \bar{2}\ 0]$
$\begin{bmatrix} 2 & 1 & \bar{1} \\ 0 & 2 & \bar{2} \\ 0 & 1 & 1 \end{bmatrix}$	$(110)_\beta[\bar{1}11]_\beta$	1	$(011)_\beta//(0001)_{\alpha'}, [1\bar{1}1]_\beta/[11\bar{2}0]_{\alpha'}$	$(\overline{0.715}\ \overline{0.493}\ 0.495)_\beta$	$[0.777\ \overline{0.435}\ 0.455]_\beta$	B	A
	$(\bar{1}10)_\beta[111]_\beta$	2	$(011)_\beta//(0001)_{\alpha'}, [11\bar{1}]_\beta/[11\bar{2}0]_{\alpha'}$	$(0.715\ \overline{0.493}\ 0.495)_\beta$	$[\overline{0.777}\ \overline{0.435}\ 0.455]_\beta$	A	B
$\begin{bmatrix} \bar{1} & 1 & \bar{2} \\ \bar{2} & 2 & 0 \\ 1 & 1 & 0 \end{bmatrix}$	$(0\bar{1}1)_\beta[111]_\beta$	3	$(110)_\beta//(0001)_{\alpha'}, [\bar{1}11]_\beta/[11\bar{2}0]_{\alpha'}$	$(\overline{0.495}\ 0.493\ \overline{0.715})_\beta$	$[\overline{0.455}\ 0.435\ 0.777]_\beta$	A	C
	$(011)_\beta[\bar{1}\bar{1}1]_\beta$	4	$(110)_\beta//(0001)_{\alpha'}, [1\bar{1}1]_\beta/[11\bar{2}0]_{\alpha'}$	$(0.495\ \overline{0.493}\ \overline{0.715})_\beta$	$[0.455\ \overline{0.453}\ 0.777]_\beta$	C	A
$\begin{bmatrix} 1 & 1 & \bar{2} \\ 2 & 2 & 0 \\ 1 & \bar{1} & 0 \end{bmatrix}$	$(10\bar{1})_\beta[1\bar{1}1]_\beta$	5	$(1\bar{1}0)_\beta//(0001)_{\alpha'}, [111]_\beta/[11\bar{2}0]_{\alpha'}$	$(\overline{0.493}\ \overline{0.495}\ 0.715)_\beta$	$[\overline{0.435}\ \overline{0.455}\ \overline{0.777}]_\beta$	B	D
	$(101)_\beta[\bar{1}11]_\beta$	6	$(1\bar{1}0)_\beta//(0001)_{\alpha'}, [11\bar{1}]_\beta/[11\bar{2}0]_{\alpha'}$	$(\overline{0.493}\ \overline{0.495}\ \overline{0.715})_\beta$	$[\overline{0.435}\ \overline{0.455}\ 0.777]_\beta$	D	B
$\begin{bmatrix} \bar{1} & 2 & 1 \\ \bar{2} & 0 & 2 \\ 1 & 0 & 1 \end{bmatrix}$	$(1\bar{1}0)_\beta[111]_\beta$	7	$(101)_\beta//(0001)_{\alpha'}, [11\bar{1}]_\beta/[11\bar{2}0]_{\alpha'}$	$(\overline{0.493}\ 0.715\ 0.495)_\beta$	$[\overline{0.435}\ \overline{0.777}\ 0.455]_\beta$	C	B
	$(110)_\beta[1\bar{1}1]_\beta$	8	$(101)_\beta//(0001)_{\alpha'}, [\bar{1}11]_\beta/[11\bar{2}0]_{\alpha'}$	$(\overline{0.493}\ \overline{0.715}\ 0.495)_\beta$	$[\overline{0.435}\ 0.777\ 0.455]_\beta$	B	C
$\begin{bmatrix} 1 & 2 & 1 \\ 2 & 0 & 2 \\ 1 & 0 & \bar{1} \end{bmatrix}$	$(011)_\beta[\bar{1}\bar{1}1]_\beta$	9	$(10\bar{1})_\beta//(0001)_{\alpha'}, [1\bar{1}1]_\beta/[11\bar{2}0]_{\alpha'}$	$(\overline{0.495}\ \overline{0.715}\ \overline{0.493})_\beta$	$[\overline{0.455}\ 0.777\ \overline{0.435}]_\beta$	D	A
	$(01\bar{1})_\beta[\bar{1}11]_\beta$	10	$(10\bar{1})_\beta//(0001)_{\alpha'}, [111]_\beta/[11\bar{2}0]_{\alpha'}$	$(0.495\ \overline{0.715}\ 0.493)_\beta$	$[0.455\ 0.777\ 0.435]_\beta$	A	D
$\begin{bmatrix} 2 & 1 & 1 \\ 0 & 2 & 2 \\ 0 & \bar{1} & 1 \end{bmatrix}$	$(10\bar{1})_\beta[1\bar{1}1]_\beta$	11	$(01\bar{1})_\beta//(0001)_{\alpha'}, [111]_\beta/[11\bar{2}0]_{\alpha'}$	$(\overline{0.715}\ 0.495\ 0.493)_\beta$	$[0.777\ 0.455\ 0.435]_\beta$	C	D
	$(101)_\beta[\bar{1}\bar{1}1]_\beta$	12	$(01\bar{1})_\beta//(0001)_{\alpha'}, [\bar{1}11]_\beta/[11\bar{2}0]_{\alpha'}$	$(\overline{0.715}\ \overline{0.495}\ \overline{0.493})_\beta$	$[0.777\ \overline{0.455}\ \overline{0.435}]_\beta$	D	C

Appendix A. 3 α' Interaction Energy (IE) map of grain 5 after 7% of deformation and IPF of the tensile direction of the parent β grains of grain 5

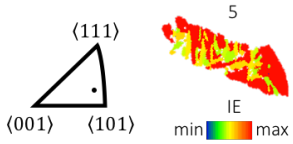

IE Ranking	1	1	2	2	3	3	4	4	4	4	5	5
Variant n°	10	9	8	3	7	4	2	1	5	6	11	12
Fraction (%)	0	96	0	0	1	1	0	1	0	1	0	0
IE	0.7	0.7	0	0	-0.1	-0.1	-0.2	-0.2	-0.2	-0.2	-0.3	-0.3

Appendix A. 4 α' martensite lattice deformation reconstruction map after 7% of deformation on a completely reoriented grain (grain 1) and a not reoriented grain (grain 8)

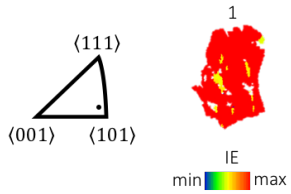

IE Ranking	1	1	2	2	3	3	4	4	4	4	5	5
Variant n°	10	9	8	7	2	1	11	12	3	4	5	6
Fraction (%)	0	96	0	0	1	1	0	1	0	1	0	0
IE	9	9	0	0	-2	-2	-2	-2	-4	-4	-4	-4

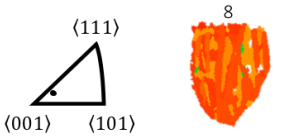

IE Ranking	1	1	1	1	2	2	2	2	3	3	4	4
Variant n°	10	9	2	1	8	11	7	12	3	4	5	6
Fraction (%)	6	25	0	41	18	8	0	1	0	0	1	0
IE	6	6	6	6	3	3	2	2	-9	-9	-10	-10

Appendix A. 5 Calculation of the α' martensite lattice deformation

The strain along the tensile direction induced by the transformation of a parent β grain into a CV i among the 6 possible is given by:

$$\varepsilon_i = T^t \, \varepsilon^{(i)} T$$

T is the tensile direction defined as a columnar vector in the coordinate system of the β phase. $\varepsilon^{(i)}$ is the lattice deformation matrix of the CV i given by T. Inamura et al. [35]. The 6 $\varepsilon^{(i)}$ are explicitly shown in Table 3.

Table 3 Lattice deformation matrices of the CVs

$$\varepsilon^{(1)} = \begin{pmatrix} \eta_1 & 0 & 0 \\ 0 & \frac{\eta_2+\eta_3}{2} & \frac{\eta_2-\eta_3}{2} \\ 0 & \frac{\eta_2-\eta_3}{2} & \frac{\eta_2+\eta_3}{2} \end{pmatrix} \qquad \varepsilon^{(4)} = \begin{pmatrix} \frac{\eta_2+\eta_3}{2} & 0 & -\frac{\eta_2-\eta_3}{2} \\ 0 & \eta_1 & 0 \\ -\frac{\eta_2-\eta_3}{2} & 0 & \frac{\eta_2+\eta_3}{2} \end{pmatrix}$$

$$\varepsilon^{(2)} = \begin{pmatrix} \eta_1 & 0 & 0 \\ 0 & \frac{\eta_2 + \eta_3}{2} & -\frac{\eta_2 - \eta_3}{2} \\ 0 & -\frac{\eta_2 - \eta_3}{2} & \frac{\eta_2 + \eta_3}{2} \end{pmatrix} \qquad \varepsilon^{(5)} = \begin{pmatrix} \frac{\eta_2 + \eta_3}{2} & \frac{\eta_2 - \eta_3}{2} & 0 \\ \frac{\eta_2 - \eta_3}{2} & \frac{\eta_2 + \eta_3}{2} & 0 \\ 0 & 0 & \eta_1 \end{pmatrix}$$

$$\varepsilon^{(3)} = \begin{pmatrix} \eta_1 & 0 & 0 \\ 0 & \frac{\eta_2 + \eta_3}{2} & -\frac{\eta_2 - \eta_3}{2} \\ 0 & -\frac{\eta_2 - \eta_3}{2} & \frac{\eta_2 + \eta_3}{2} \end{pmatrix} \qquad \varepsilon^{(6)} = \begin{pmatrix} \frac{\eta_2 + \eta_3}{2} & -\frac{\eta_2 - \eta_3}{2} & 0 \\ -\frac{\eta_2 - \eta_3}{2} & \frac{\eta_2 + \eta_3}{2} & 0 \\ 0 & 0 & \eta_1 \end{pmatrix}$$

η_1, η_2, η_3 are the principal strains phase transformation of β to α' given as:

$$\eta_1 = \frac{a_0 - a_b}{a_b}$$

$$\eta_2 = \frac{b_0 - \sqrt{2}a_b}{\sqrt{2}a_b}$$

$$\eta_3 = \frac{c_0 - \sqrt{2}a_b}{\sqrt{2}a_b}$$